Polymer 49 (2008) 5549–5563

Contents lists available at ScienceDirect

Polymer

journal homepage: www.elsevier.com/locate/polymer

# Radiation tolerance in polymeric dielectrics by small molecule doping, Part II: Thermodynamic and kinetic parameters

Robert J. Klein [a,**], Shannon M. Cole [b], Michael E. Belcher [b], John L. Schroeder [a], Phillip J. Cole [c], Joseph L. Lenhart [a,*]

[a] Organic Materials Department (1821), Sandia National Laboratories, Albuquerque, NM 87185, USA
[b] Organic Materials Department (2453), Sandia National Laboratories, Albuquerque, NM 87185, USA
[c] NNSA Satellite Programs (5732), Sandia National Laboratories, Albuquerque, NM 87185, USA

ARTICLE INFO

*Article history:*
Received 24 June 2008
Received in revised form 27 August 2008
Accepted 28 August 2008
Available online 18 September 2008

*Keywords:*
Radiation
Polymer
Conductivity

ABSTRACT

The doping of Mylar® film (composed of semicrystalline poly(ethylene terephthalate)) with small molecule electron traps results in a high-quality dielectric film with excellent radiation tolerance. Fluorenones with electron-withdrawing substituents, doped from ethylene glycol, are excellent candidates to provide this radiation tolerance. Utilizing theories for diffusion and partitioning, this paper extracts kinetic and thermodynamic information from the doping process. Diffusion is significantly retarded, and partitioning significantly enhanced, upon the addition of polar substituents to the dopant molecule; dopant size has a minor impact. Diffusivity corrections due to tortuous paths around the crystallites are accounted for. Additionally, it was found that the solubility parameters, in combination with estimations for the local interaction volumes, provide an excellent method to predict trends in the equilibrium doping behavior via the $\chi$ parameter and hydrogen bonding-modified Flory–Huggins theory. Based on this method, estimations are given for the number of hydrogen bonds between ethylene glycol and dopant molecules.



## 1. Introduction

Radiation-induced conductivity (RIC) can damage the performance of organic dielectrics in environments containing radiation. Depending on the specific application environment, the radiation may include X-rays, $\gamma$-rays, protons, or high-energy electrons. The interaction of these types of high-energy radiation with an organic material leads to the formation of mobile electron–hole pairs, which can result in high electrical loss and poor dielectric performance. Unfortunately, high-quality organic films that also possess radiation tolerance are not commonly available from commercial sources. One route to produce such films is to dope commercial films with electron or hole traps. As described in the first paper on this topic, Kurtz et al. [1,2] introduced poly(ethylene terephthalate) (PET) doped with trinitrofluorenone (TNF) to simultaneously provide radiation tolerance while retaining the other properties desired from an organic dielectric. Recent work [3,4] extended the method of doping PET with small molecule electron traps to many other small molecule dopants. The introduction of paper I contains further background on RIC and small molecule doping of polymers [5].

Here we continue the work presented in the first paper by developing a physical model to fit the results obtained for doping Mylar® (PET) with a series of dopants. The polymer is doped by immersing the film in a solvent–dopant solution at elevated temperatures, and relying on the chemical potential difference between the dopant in the polymer and the dopant in the solvent to drive diffusion. A physical model based on this concept allows extraction of the parameters characterizing the kinetics and thermodynamics that lead to dopant impregnation in the PET films, including the diffusivity of the dopant in the Mylar® film, the partition coefficient for the dopant equilibrating between the solvent and the polymer, and the activation energies of both parameters. Diffusion is a relatively simple mechanism to address, but partitioning of dopant – based on chemical potentials and therefore $\chi$ parameters and solubilities – is considerably more complex, as will be described in Section 2. The fluorenone-based dopants include TNF, dinitrofluorenone (DNF), nitrofluorenone (NF), fluorenone (F), and cyanofluorenone (CF), doped from

* Corresponding author. Current address: US Army Research Laboratory, Weapons and Materials Research Directorate, Aberdeen Proving Ground, MD 21005-5069, USA. Tel.: +1 410 306 1940; fax: +1 410 306 0676.
** Corresponding author. Current address: Luna Innovations, Charlottesville, VA 22903, USA. Tel.: +1 434 220 2517.
*E-mail addresses:* kleinr@lunainnovations.com (R.J. Klein), joseph.lenhart1@arl.army.mil (J.L. Lenhart).

0032-3861/$ – see front matter © 2008 Published by Elsevier Ltd.
doi:10.1016/j.polymer.2008.08.069

a homogeneous solution of ethylene glycol (EG). Data for nitropyrene (NP) were also obtained in order to compare a dopant of larger size but similar functionality to NF. (See Fig. 1 for chemical structures of dopants and polymer.) In addition, various data sets using alternate solvents and dopants were collected to confirm the validity of the physical model assembled here. Dopant concentrations in the films were obtained as a function of dopant chemistry, solvent chemistry, doping temperature, and doping time. Most importantly, fitting of the data leads to meaningful information about the impact of solvent, polymer, and dopant chemistry on the diffusivity and equilibrium concentrations. These results thereby enable predictions to be made for a wide variety of alternative chemistries based on size and functional group interactions.

## 2. Theory: partitioning and diffusion

Initially, we hypothesized that adsorption of the dopant to the film surface provided the concentrating mechanism to drive further diffusion into the bulk film [3]. This was based in part on the fact that the dopant is typically concentrated in the film at levels exceeding the solution concentration. (Concentration in the film will be denoted by $C_M$ and concentration in the solution by $C_S$.) However, the balance of chemical potentials can also lead to partitioning of the dopant at higher concentrations in the film than in solution, as supported by many previous studies: in particular, those of Dill and De Young provide excellent theoretical insight [6,7]. Two pieces of evidence that *oppose* the importance of adsorption were presented in paper I [5]: (1) the very minor effect of a 2 min UV–ozone treatment on $C_M$ (<3% increase: see Table 3 in paper I); and (2) the linear relationship between $C_M$ and $C_S$ that persisted even to very high levels of $C_M$ (Fig. 9f in paper I). UV–ozone treatment will increase concentration of oxygen groups into the film surface [8,9], which would increase the number of interaction sites between dopant and polymer and, if adsorption played a role, therefore increase the equilibrium dopant concentration. Regarding the linearity at high concentrations, calculation of the maximum geometric packing density of TNF molecules indicates that near 200 mol/m$^3$ steric limitations would lead to downward curvature in $C_M$ ($C_S$). There is also strong evidence for the influence of chemical potential on $C_M$ in the excellent correlations between predicted and experimental partition coefficients, presented later in this paper.

Therefore we will model the concentration data using a combination of partition and diffusion relationships. The film is much thinner (ca. 300 times) in cross-section than in width or height, which reduces the situation to a single dimension where the dopant only diffuses along the *x*-direction. The schematic in Fig. 2 illustrates the physical situation and the parameters of interest. The chemical potentials $\mu_d^P$ and $\mu_d^S$ are defined as those of the dopant in the polymer and solvent, respectively.

### 2.1. Partitioning of the dopant from solvent to polymer

For a two phase system in equilibrium, temperature *T*, pressure *P*, and fugacity *f* (or "residual" chemical potential) are equal [10,11]. This provides a means to treat partitioning of a solute (denoted by the subscript 1) from phase I into phase II, at constant *T* and *P*. This is governed by [11]

$$\overline{f}_1^{\mathrm{I}}\left(T,P,x_1^{\mathrm{I}}\right) = \overline{f}_1^{\mathrm{II}}\left(T,P,x_1^{\mathrm{II}}\right) \tag{1}$$

where *x* is mole fraction. The activity coefficient $\gamma_1$ is defined by the relation

$$\overline{f}_1^{\mathrm{I}}\left(T,P,x_1^{\mathrm{I}}\right) = x_1^{\mathrm{I}}\gamma_1^{\mathrm{I}}\left(T,P,x_1^{\mathrm{I}}\right)f_1(T,P) \tag{2}$$

Substituting Eq. (2) into Eq. (1), the fugacities of the pure solute $f_1$ cancel, leaving:

$$x_1^{\mathrm{I}}\gamma_1^{\mathrm{I}}\left(T,P,x_1^{\mathrm{I}}\right) = x_1^{\mathrm{II}}\gamma_1^{\mathrm{II}}\left(T,P,x_1^{\mathrm{II}}\right) \tag{3}$$

We can then define a mole fraction partition coefficient $K_x$ as

$$K_x = \frac{x_1^{\mathrm{I}}}{x_1^{\mathrm{II}}} = \frac{\gamma_1^{\mathrm{II}}(T,P,x_1^{\mathrm{II}})}{\gamma_1^{\mathrm{I}}(T,P,x_1^{\mathrm{I}})} \tag{4}$$

We want to apply Eq. (4) to the dopants under consideration. In order to establish *a priori* estimates for $K_{\mathrm{dopant}}(T)$, we need values for $\gamma$ for the dopant in the solvent and the dopant in the polymer. Throughout this paper, we utilize concentrations rather than mole fractions, so the concentration partition coefficient for the dopant $K_C$ is obtained from

$$C_M^{\mathrm{eq}} = K_C C_S \tag{5}$$

where it is important to distinguish $K_C$ as different than $K_x$. (The "eq" superscript denotes the equilibrium value of $C_M$.) $K_c$ and $K_x$ are related by a conversion factor that depends on the molar volume of the solvent and the polymer, and this will be introduced explicitly later. For the moment we continue with $K_x$:

$$K_x = \frac{x_d^P}{x_d^S} = \frac{\gamma_d^S}{\gamma_d^P} \tag{6}$$

where the scripts d, P, and S indicate dopant, polymer, and solvent, respectively. For example, $x_d^P$ denotes the mole fraction of dopant in the polymer phase.

#### 2.1.1. Flory–Huggins theory

There are many models that have been developed to treat activity coefficients $\gamma_i$, especially as a function of mole fraction. These models include [11–14]: regular solution theory (developed by Hildebrand), which also encompasses van Laar theory; Flory–Huggins theory, which expands regular solution theory to cases where the volumes of components differ; lattice–fluid model, which starts with Flory–Huggins theory and adds contributions for the thermodynamic properties of the pure components; empirical equations with multiple fitting constants such as the Margules equation, the Redlich/Kister expansion, and the Wilson equation; Henry's law, which assumes a linear dependence of $\gamma_i$ on $x_i$ at small $x_i$; and empirically-based group contribution models that are based on libraries of data for molecular functional groups, and generally include the UNIQUAC (universal quasichemical) model developed by Adams, Praus-nitz, and others, and the UNIFAC (UNIquac functional group activity coefficient) model, an advancement on the UNIQUAC model. Out of these many models, there are very few, however, that have established sufficient libraries of information to *a priori* predict the activity coefficients for a chemical mixture: only regular solution theory, Flory–Huggins, lattice–fluid, and UNIFAC have no adjustable parameters (although the latter three still involve coefficients based on a library of experimental data). We will apply Flory–Huggins (F–H) theory, lattice–fluid (LF) theory (with some modifications based on hydrogen bonding), and UNIFAC to obtain estimates for $\gamma_i$ and compare these with experiment. The F–H model provides [11]

$$\ln\gamma_1 = \ln\frac{\phi_1}{x_1} + (1 - 1/m_{2.1})\phi_2 + \chi\phi_2^2 \tag{7}$$

and

$$\ln\gamma_2 = \ln\frac{\phi_2}{x_2} + (m_{2.1} - 1)\phi_1 + \chi\phi_1^2 \tag{8}$$

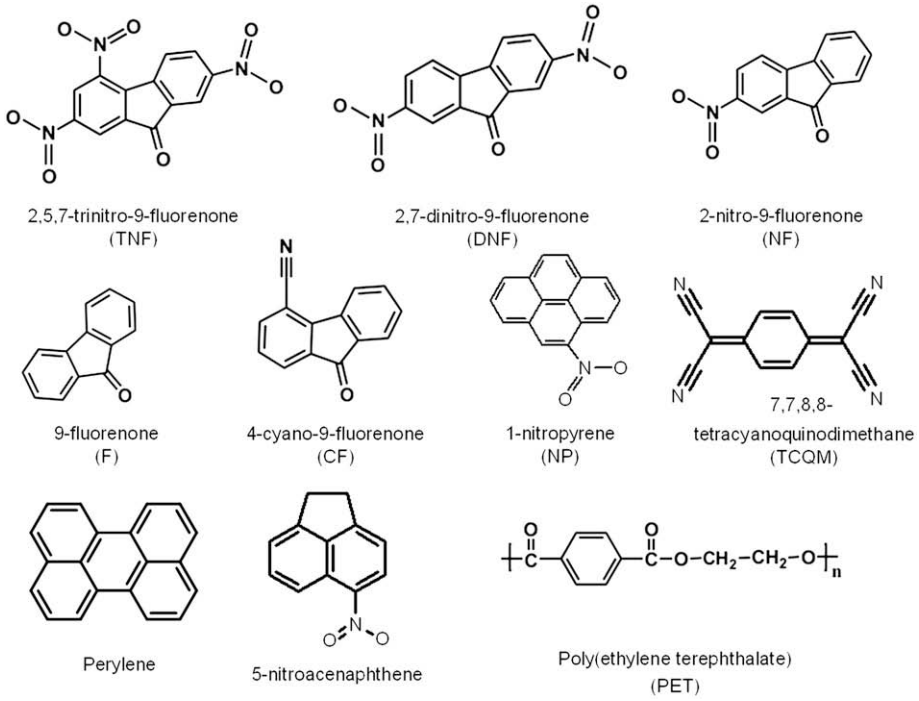


**Fig. 1.** Structures of the dopants and polymer under investigation in this study.

where component 1 indicates the smaller molecule and component 2 the larger. Here we follow the notations used by Sandler [11], and volume fractions $\phi$ are obtained from

$$\phi_1 = \frac{x_1}{x_1 + m_{2.1}x_2} \tag{9}$$

$$\phi_2 = \frac{m_{2.1}x_2}{x_1 + m_{2.1}x_2} \tag{10}$$

and the molar volume ratio from

$$m_{2.1} = \frac{v_2}{v_1} \tag{11}$$

where $v_i$ indicates the molar volume of component *i*.

According to the original theory, the first two terms in Eq. (7) or Eq. (8) are based on entropic considerations, and the term containing $\chi$ is due to enthalpic interactions. However, research into real mixtures has shown that $\chi$ itself contains both entropic and enthalpic parts [15]. It is important to note that relationships developed to calculate $\chi$ (discussed below) are based on experimental data, and therefore incorporate interactions that go beyond what the original F–H theory intended.

Continuing with the F–H model, equations for the dopant in polymer and dopant in solution can be written independently. Although the molecular weight of the Mylar® is unknown, we proceed by assuming a molecular weight $M_n \approx 10{,}000$ g/mol, which is equivalent to a degree of polymerization $N = M_n/M_0 \approx 52$. Note that *in this case,* if a mer in the chain is used as the basis for calculations instead of a polymer chain, the calculations end up being equivalent by virtue of a factor – the degree of polymerization $N$ – added to both sides of Eq. (6). The parallel calculation in terms of mers is given below. Utilizing the full polymer chain as a basis, the PET chain is larger than the dopant, and the dopant in the polymer follows Eq. (7):

$$\ln \gamma_d^P = \ln \frac{\phi_{d.P}}{x_{d.P}} + (1 - 1/m_{P.d})\phi_P + \chi_d^P \phi_P^2 \tag{12}$$

We use subscripts d.P to indicate dopant in the polymer, d.S for dopant in the solvent, P for the polymer phase (which is predominantly polymer), and S for the solvent phase (which is predominantly solvent). Under the conditions of the present experiment, volume fractions are extremely small and the polymer and dopant can be considered to be in their pure state on a volumetric basis. For an order of magnitude estimate, at the highest concentrations used here ($C_S = 40$ mol NP/m$^3$ EG, $C_M = 350$ mol NP/m$^3$ PET), $x_d^S = 0.0022$ mol NP/mol EG and $x_d^P = 0.072$ mol NP/(mol PET + mol NP). As will be discussed later, $m_{d.S} \approx 5$ and $m_{P.d} \approx 52$, giving maximum values for $\phi_d^S$ and $\phi_d^P$ of 0.01 and 0.0004, respectively.

Taking the exponential of both sides and assuming $\phi_P \approx 1$ yields:

$$\gamma_d^P = \frac{\phi_{d.P}}{x_{d.P}} \exp(1 - 1/m_{P.d}) \exp\left(\chi_d^P\right) \tag{13}$$

For the dopant in the solution, we must also use F–H theory, since the molar volumes of the dopant (e.g., fluorenone) are significantly larger than that of the solvent (EG). Using Eq. (8), similar steps follow as for the dopant in polymer to give:

$$\gamma_d^S = \frac{\phi_{d.S}}{x_{d.S}} \exp(m_{d.S} - 1) \exp\left(\chi_d^S\right) \tag{14}$$

Therefore we can construct an equation for the partition coefficient:

$$K_x = \frac{x_d^P}{x_d^S} \approx \frac{\gamma_d^S}{\gamma_d^P} \approx \frac{(\phi_{d.S}/x_{d.S}) \exp(m_{d.S} - 1) \exp\left(\chi_d^S\right)}{(\phi_{d.P}/x_{d.P}) \exp(1 - 1/m_{P.d}) \exp\left(\chi_d^P\right)} \tag{15}$$

We can further simplify $\phi_{d.S}/x_{d.S}$ and $\phi_{d.P}/x_{d.P}$ using Eqs. (9) and (10). Modifying Eq. (15) gives

$$K_x = \frac{(m_{d.S}/x_S + m_{d.S}x_{d.S})\exp(m_{d.S} + 1/m_{P.d} - 2)\exp\left(\chi_d^S\right)}{(1/x_{d.P} + m_{P.d}x_P)\exp\left(\chi_d^P\right)} = \frac{m_{d.S}(x_{d.P} + m_{P.d}x_P)}{x_S + m_{d.S}x_{d.S}}\exp(m_{d.S} + 1/m_{P.d} - 2)\exp\left(\chi_d^S - \chi_d^P\right) \quad (16)$$

Several simplifying assumptions allow the removal of the dependence on concentrations: $x_S \gg m_{d.S}x_{d.S}$, $x_S \approx 1$, $x_P \gg m_{d.P}x_{d.P}$, and $x_P \approx 1$. We finally have

$$K_x = m_{d.S}m_{P.d}\exp(m_{d.S} + 1/m_{P.d} - 2)\exp\left(\chi_d^S - \chi_d^P\right) \quad (17)$$

Eq. (17) is essentially equivalent to the relations described in Wakahayashi et al. [16] and De Young and Dill [7] for partitioning of solutes between immiscible phases, for dispersive interactions only. For comparison, if the mer in a chain is used instead of polymer chain, $K_x$ becomes

$$K_x = \frac{x_d^{P\prime}}{x_d^S} = \frac{m_{d.S}}{m_{d.P}}\exp(m_{d.S} - m_{d.P})\exp\left(\chi_d^S - \chi_d^P\right) \quad (18)$$

where by virtue of $x_d^{P\prime} = x_d^P/N$, $m_{d.P} = N/m_{P.d}$, and $m_{d.P} \approx 2$, Eq. (18) is numerically equivalent to Eq. (17) for the values of $m$ in this study.

*2.1.2. Corrections to Flory–Huggins theory*

A significant amount of research has accumulated since the F–H theory was initially proposed, correcting for inconsistencies between the original theory and new experimental data. In particular, F–H theory neglects free volume effects as a larger molecule mixes with a smaller one [17], and also omits the equation of state properties of the pure species [13]. This has led to a lattice–fluid (LF) model that contains the original F–H theory and an additional term based on reduced densities, reduced pressures, and reduced temperatures. Calculation of these quantities is beyond the scope of this paper, although the corrections will ultimately add an additional, non-temperature-dependent term to Eq. (17): see Sanchez and Lacombe for more details [13]. This term is near unity under the experimental conditions here, and so will be neglected.

Polar and hydrogen bonding interactions also provide an additional contribution to the chemical potential. The complexity of the theory increases significantly with these additions: Panayiotou and Sanchez [14] and Graf et al. [18] develop a theoretical basis to account for hydrogen bonding in particular. Their models require explicit knowledge of the Gibbs free energies of the components to fully calculate these terms. It is nonetheless helpful to examine the influence of hydrogen bonding, which is represented for the hydrogen bonding contribution to the chemical potential $\Delta\mu_{1,H}$ of the proton accepting species [14] by

$$\frac{\Delta\mu_{1,H}}{RT} = r_1\nu_H - 2a\ln\frac{2ax_1}{2ax_1 - r\nu_H} \quad (19)$$

where species 1 contains $a$ proton acceptor groups per molecule (and species 2 contains two proton donating groups per molecule), $r_1$ and $r$ are size factors, and $r\nu_H$ is the size-adjusted molar volume of hydrogen bonds. In our particular case, the solvent (ethylene glycol) hydrogen bonds with the dopant, but from inspection of the chemical structure there is no capacity for hydrogen bonding between the polymer and dopant. Therefore the influence of hydrogen bonds can be introduced as a contribution to the solvent activity coefficient using $\ln\gamma_1 = \Delta\mu_1/RT$:

$$\gamma_d^{S(H)} = \frac{\exp(r_1\nu_H)}{\exp(2a\ln(2ax_1/2ax_1 - r\nu_H))} \quad (20)$$

where the new dopant in solvent activity coefficient $\gamma_d^S$ will equal the original multiplied by $\gamma_d^{S(H)}$.

Making the approximations that $r_1\nu_H$ is small and $r\nu_H \approx ax_1$ (the latter is extreme but very helpful for simplification), Eq. (20) reduces to:

$$\gamma_d^{S(H)} \approx \exp(-2a) \quad (21)$$

This will allow for approximations of the number of hydrogen bonds per dopant molecule. Note that there is no temperature dependence to Eqs. (20) and (21), which is somewhat unphysical since the strength of a hydrogen bond decreases with increasing temperature [19]. This will add additional temperature dependence to the "pre-exponential" term, leading to curvature in Arrhenius plots as a function of temperature. However, as will be discussed later, the data obtained in this report follow the Arrhenius relation well, demonstrating that within the temperature range investigated here H-bonding is relatively stable.

*2.1.3. Treatment of the $\chi$ parameters*

It is possible to estimate $\chi$ using the solubility parameters $\delta_i$:

$$\chi_{AB} = \frac{\nu_m(\delta_A - \delta_B)^2}{RT} \quad (22)$$

where solubility parameters are defined for pure components A and B. This relationship has the firmest theoretical background for non-polar mixtures interacting mainly by dispersion forces [15], but is often extended to polar mixtures (especially for industrial formulations). $\nu_m$ denotes the interaction site volume per mole. It is important to note that the solubility parameters are obtained either directly from experimental data on vaporizing liquids or from group contribution methods that are derived from experimental data, and therefore the influence of the dipolar nature of the molecules is intrinsically accounted for.

Solubility parameters $\delta$ are based on chemical structure of the molecule under consideration. It was realized by Hildebrand and Scatchard that values of $\delta$ strongly correlate with internal pressures, or cohesive energy densities, of liquids [17,20]. Solubilities can therefore be obtained from the cohesive energy density $E$ as

$$\delta = \left(\frac{E}{V}\right)^{1/2} \quad (23)$$

where $V$ is the molecular molar volume. Cohesive energy densities can be obtained from heats of vaporization for pure liquids. Work by Small [21] extended Eq. (23) by considering $E$ and $V$ as quantities that could be constituted by group contributions from specific functional groups. Eq. (23) is rewritten for a particular species as [20–22]

$$\delta = \left(\frac{\sum_i E_i}{\sum_i V_i}\right)^{1/2} \quad (24)$$

where all atoms, bonds, and functional groups $i$ in the molecule are accounted for. Values for $E_i$ and $V_i$ were developed by Small and many other groups using slightly different methods, but it appears that the most frequently-used values at the present time are those compiled by Fedors [22,23] for small molecules, and by Hoftyzer and Van Krevelen [20] for polymers. For this work, these two correlations are utilized where directly-determined solubility parameters are not available; for solvents, the solubility parameters

listed in the most recent work by Hansen and Barton [24,46] are used.

*2.1.4. Temperature dependence of the F–H model*

Eq. (17) reveals that the exponential term containing the $\chi$ parameters is the only term dependent on temperature. Therefore the F–H model can be broken into pre-exponential and exponential terms, and the latter term (containing the temperature dependence) is written:

$$K_x \sim \exp\left[\frac{v_m^{d,S}(\delta_S-\delta_d)^2 - v_m^{d,P}(\delta_P-\delta_d)^2}{RT}\right] \tag{25}$$

$$K_x \sim \exp\left[\frac{E_a}{RT}\right] \tag{26}$$

where $E_a$ is thereby defined by the numerator of the exponential. Thus we obtain an estimation of the partition coefficient activation energy $E_a$ that depends on the $\chi$ parameters of the dopant, solvent, and polymer.

*2.1.5. Estimation of activity coefficients by UNIFAC*

The other method we will utilize to obtain *a priori* estimates of activity coefficients $\gamma_i$ is UNIFAC, which is a development from the original UNIQUAC (universal quasichemical) model. UNIQUAC is derived from statistical mechanics in an attempt to follow the local composition changes that result from both size and energy differences when species are mixed, and is composed of a "combinatorial" and a "residual" term [11]. The combinatorial term is calculated from volume and surface area parameters developed for a wide variety of functional groups. However, the residual term in UNIQUAC, which is based on interaction energies, contains two adjustable parameters.

The UNIFAC model is slightly different from UNIQUAC, in that it subdivides the interactions into functional group interactions (regardless of which species is involved) rather than first adding all the functional group contributions on each molecule and then finding interactions between molecules, as in the UNIQUAC model. The UNIFAC model is also based on a combinatorial and a residual terms, which are based on the same volume and surface parameters as UNIQUAC, with additional parameters representing binary interactions between functional groups. There have been several iterations of and modifications to the original work by Fredenslund et al. [25] The mathematics are complex and will not be presented here: literature by Fredenslund et al. [26,27] and others [11,28] provide more details. We will utilize a computer program written by Sandler [11], based on the fourth revision of the UNIFAC model [29], for calculations of activity coefficients as a function of chemistry and temperature. There are two faults of this specific model: it does not account for either the impact of hydrogen bonding or chain connectivity in polymer solutions.

### 2.2. Diffusion of dopant into the film

Diffusion from both sides of the film is considered as a simple mass transport process. Two simplifying assumptions must be made: the dopant is not consumed by any chemical changes within the film and diffusivity of the dopant $D$ is independent of the concentration of dopant. The latter assumption has been examined in other systems [30,31] and in the case of the dopant being a good plasticizer (such as di-2-ethylhexyl phthalate in poly(vinyl chloride)), as the concentration of plasticizer rises above 1 wt% $D$ increases by orders of magnitude [32]. In this case, the dopants are not good plasticizers, and concentrations of the dopants in the Mylar® are typically <1 mol%; the exception is for CF at high solution concentrations where $C_M$ may reach 6 mol dopant/mol PET mers ($\sim$400 mol/m$^3$). Even when doped to these levels, however, the $T_g$ is virtually unchanged from that of the neat Mylar®: see Fig. 6 of paper I [5].

Combining the mass balance taken around the film boundary and Fick's law for diffusion of the dopant [31,33] results in

$$D\frac{\partial^2 C_M}{\partial x^2} = \frac{\partial C_M}{\partial t} \tag{27}$$

where boundary conditions include $C_M(x,t=0)=0$, $C_M(x=1/2,L) = C_M(x=-1/2,L) = C_M^{eq}$, and $C_M(x,t\to\infty) = C_M^{eq}$, where $C_M^{eq}$ refers to the equilibrium concentration of dopant in the Mylar®.

Eq. (27) can be solved by introducing dimensionless parameters, integrating by parts, and applying the boundary conditions [33] to produce:

$$C_M(x,t) = C_M^{eq}\left\{1 - 2\sum_{n=0}^{\infty}\frac{(-1)^n}{(n+1/2)\pi}\exp \times\left[-(n+1/2)^2\pi^2\frac{Dt}{(L/2)^2}\right]\cos\left[(n+1/2)\pi\frac{x}{L/2}\right]\right\} \tag{28}$$

### 2.3. Combined model and simulated results

As $C_M^{eq}$ is determined by Eq. (5), the time-dependent expression for $C_M$ is composed of the combination of Eqs. (5) and (28):

$$C_M(x,t) = K_C C_S\left\{1 - 2\sum_{n=0}^{\infty}\frac{(-1)^n}{(n+1/2)\pi}\exp \times\left[-(n+1/2)^2\pi^2\frac{Dt}{(L/2)^2}\right]\cos\left[(n+1/2)\pi\frac{x}{L/2}\right]\right\} \tag{29}$$

The experimental partition coefficient $K_C$ can then be compared to values determined theoretically from the Flory–Huggins and UNIFAC methods. There are, as described separately above, two important limitations to the use of Eq. (29): (1) no chemical changes occur in the form of reactions between dopant, solvent, and polymer; and (2) diffusivity is independent of dopant concentration and the solvent does not swell the polymer film. Simulated results for $C_M(x,t)$ are shown in Fig. 3 for a time series. Values of $K_C$, $C_S$, and $D$ used in the model were chosen to represent values typical of the experimental data. As time increases, the dopant diffuses into the film creating parabolic concentration profiles, and at long times reaches the constant value $C_M^{eq} = K_C C_S$ over the entire thickness $-L/2 \le x \le L/2$.

## 3. Experimental

### 3.1. Materials

2-Nitro-9-fluorenone (NF, 99%), 2,7-dinitro-9-fluorenone (DNF, 97%), 2,5,7-trinitro-9-fluorenone (TNF, 99%, Sandia National Laboratories), 9-fluorononone (F, 99%), 4-cyano-9-fluorononone (CF, 99.5%), 1-nitropyrene (NP, 99%), 7,7,8,8-tetracyanoquinodimethane (TCQM, 99%), anthracene (99%), phenazine (99%), perylene (99%), 5-nitroacenaphthene (NAN, 99%), isopropanol (99.9%), acetone (99.5%), toluene (99.8%), bis(2-ethylhexyl) sebacate (BEHS, 97%), dibutyl phthalate (DBP, 99%), methyl ethyl ketone (MEK, 99%), dimethyl formamide (DMF, 99.8%), dimethyl sulfoxide (DMSO, 99.9%),

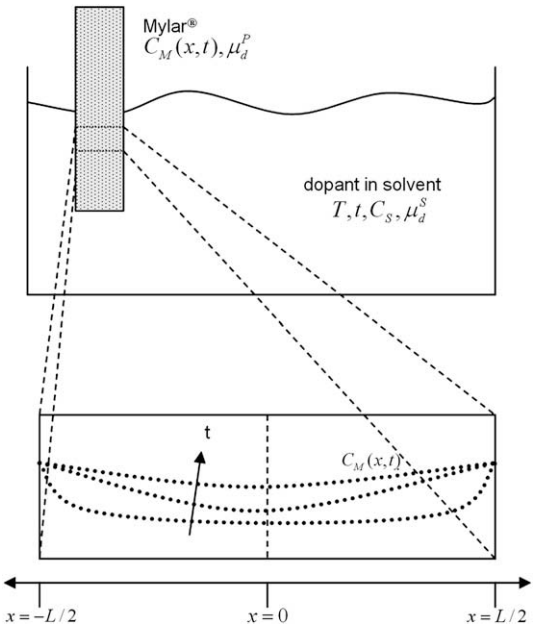


**Fig. 2.** Schematic of the dipping process used to impregnate PET with dopant. Independent variables include temperature $T$, doping time $t$, and dopant concentration in the solvent $C_S$, all of which determine the final dopant concentration in the PET film ($C_M$). The expanded view illustrates the expected concentration profiles over time $t$ as dopant diffuses through the film along the $x$-direction.

glycerin (99.5%), and ethylene glycol (EG, electronic grade, Air Products) were obtained from Fisher Scientific or Acros Organics unless otherwise noted. Mylar® C capacitor grade poly(ethylene terephthalate) (PET) film 12.9 μm thick was obtained from DuPont. Chemical structures of the dopants and polymer are shown in Fig. 1.

### 3.2. Film preparation and characterization

Mylar® films were first wiped with isopropanol to clean the film surface. Films were then held in heated EG solutions prepared with the proper concentration of small molecule dopant for specified times. Solution temperature $T$ and solution concentration $C_S$ were carefully controlled over the length of the doping time $t$ (Fig. 2). The films were then removed, rinsed in isopropanol, acetone, and toluene, and annealed under vacuum at 82 °C for at least 12 h. For each dopant, concentration calibration curves were established by ultraviolet–visible (UV–vis) spectroscopy (PerkinElmer, Lambda 950) in transmission mode using solutions of known concentrations. Further details on UV–vis analysis are given in paper I [5].

The range of temperatures and solution concentrations chosen for TNF, DNF, NF, CF, F, and NP were limited by three factors: (1) the solubility of the dopant in EG, (2) the thermal degradation over time of the dopant, and (3) very low diffusivities at temperatures below 100 °C. For example, TNF and CF precipitate below 100 °C at concentrations above 1 mol/m$^3$. Most dopants degrade after several hours at 150 °C and some degrade after a few days at 135 °C (observed as a gradual darkening in the solution color). The extent and chemical nature of the degradation that caused this color change was not investigated. Solutions that started to exhibit even a subtle color change were not utilized further, and replaced with fresh solutions. Doping with F was limited by the abnormally high (>10 mol/m$^3$) solution concentrations required to obtain measurable film dopant concentrations. As noted in paper I [5], below 100 °C diffusion was so slow that days were required to reach equilibrium. In addition, there were only small amounts of CF available commercially, limiting the number of samples that could be evaluated.

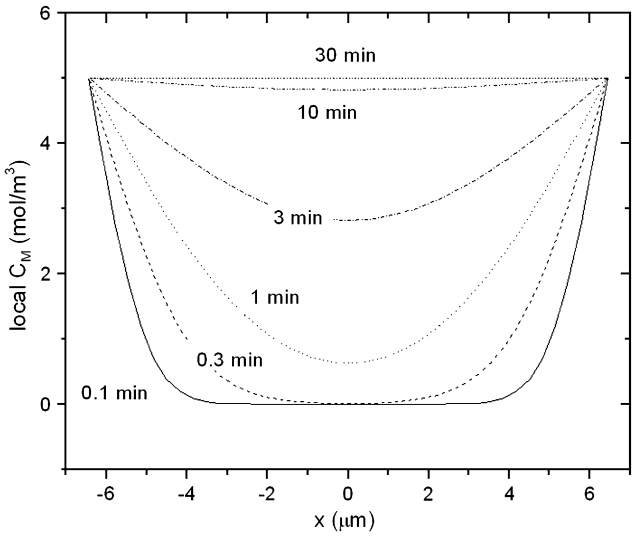


**Fig. 3.** Modeled results for $C_M$ over the range of $x$ values for $C_S = 1$ mol/m$^3$, $D$ =10−9 cm$^2$/s, and $K_C = 5$, using Eq. (29).

Differential scanning calorimetry was used to obtain the crystallinity of the Mylar® film. $\Delta H$ was measured as 36.8 ± 4.6 J/g, and using the ideal heat of fusion of 96.0 J/g from Kong and Hay [34], the crystallinity of the film was found to be 39 ± 5%.

## 4. Results and discussion

### 4.1. Fits of the data

With a physical model containing the process kinetics and thermodynamics, the fitting of experimental $C_M(t)$ data sets can proceed. Values obtained for TNF, DNF, NF, CF, F, and NP were fit as follows. The film thickness $L$ was the same for all measurements, 12.9 μm. Solution concentrations $C_S$ were defined by the prepared solution ratio of dopant to EG. For each dopant and temperature, the sum of the residuals between the experiment and the model was minimized to converge on values for $D$ and $K_C$. (i.e., $C_M(t)$ data for all available $C_S$ at a particular $T$ and for a particular chemistry were fit simultaneously.) The model applied was Eq. (29) and 95% confidence intervals for $K_C$ and $D$ were calculated based on the standard deviations:

$$\sigma_{K_C}^2 = \sigma_{C_M}^2 / \left(\frac{\partial C_M}{\partial K_C}\right)^2 \tag{30}$$

and

$$\sigma_D^2 = \sigma_{C_M}^2 / \left(\frac{\partial C_M}{\partial D}\right)^2 \tag{31}$$

where $C_M$ is determined by Eq. (29) and only the applicable data (plateau region for $K_C$ and non-plateau for $D$) were used in separate calculations of $\sigma_{K_C}$ and$\sigma_D$. The results of the fitting procedure are shown in Figs. 4–9 for the six dopants TNF, DNF, NF, CF, F, and NP, respectively. The partition–diffusion model fits all data sets extremely well, representing a wide range of times, temperatures, solution concentrations, and dopants. To illustrate the fitting quality at short times and decompress overlapping data points, Fig. 10 expands the data sets for several conditions over short times. As a rough quantification, values for the coefficient of determination $R^2$ ranged from 0.9992 for NF at 125 °C to 0.980 for CF at 135 °C.

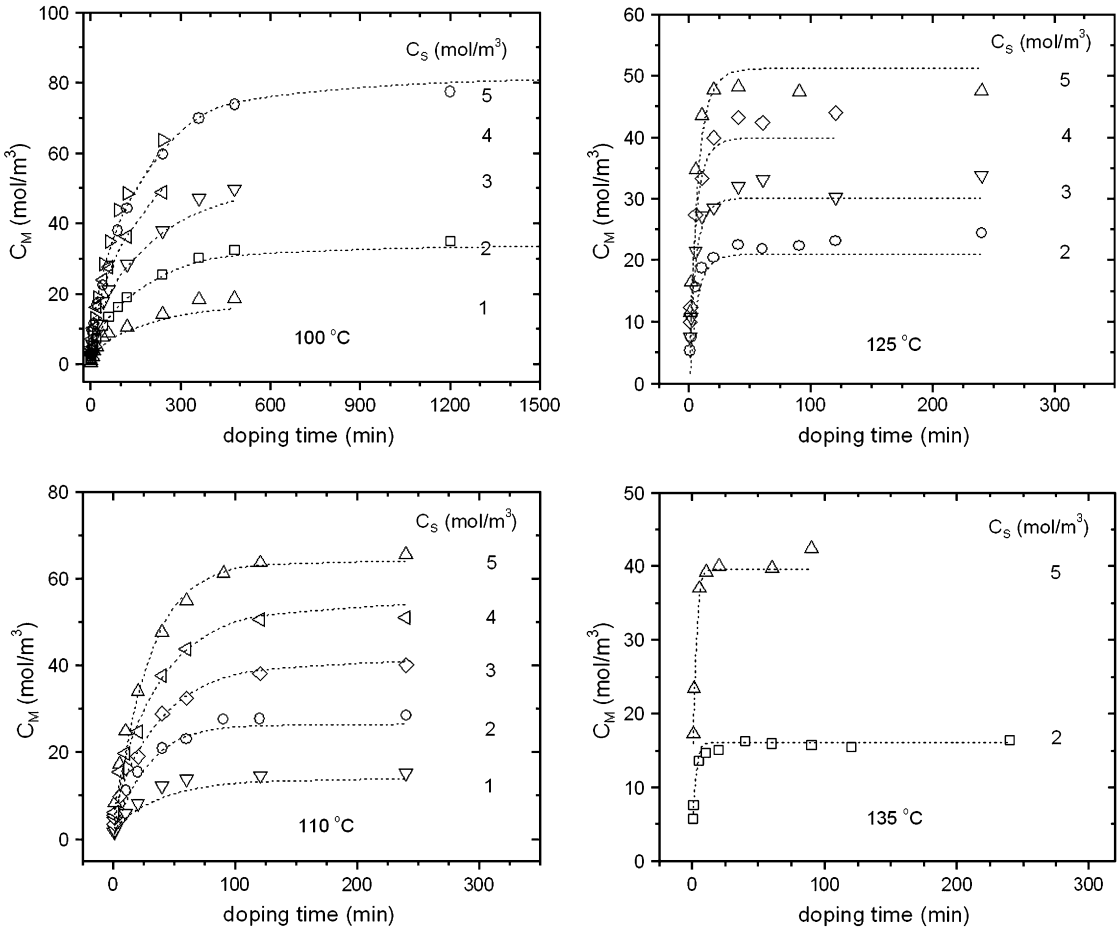


**Fig. 4.** Concentrations of TNF in Mylar® after doping at specified times, solution concentrations, and temperatures. Dashed lines indicate best-fits.

### 4.2. *Behavior of* D

With the data sets fully characterized by the physical model, we can proceed to the key parameters of the process, diffusivity $D$ and equilibrium partition coefficient for concentration $K_C$. As seen in Fig. 11 for $D$, the four dopants shown appear to follow Arrhenius behavior. The temperature of doping here is in an intermediate regime relative to the polymer $T_g^{DSC}$ between 20 and 60 °C above $T_g^{DSC}$. Diffusion through amorphous polymers (the PET under consideration is $39 \pm 5\%$ crystalline) nearly always follows Arrhenius-like behavior at temperatures far (typically $> 50$ °C) above $T_g$ [35,36]; whereas closer to $T_g$, curvature is typically seen in accordance with the Vogel–Fulcher–Tammann (VFT) model, due to cooperativity between dopant diffusion and polymer segmental motion. A wider temperature range for diffusivity may reveal VFT behavior, but with no strong evidence for curvature we will proceed with analysis in the context of Arrhenius behavior.

Within the measurement error all dopants exhibit approximately the same activation energy for diffusion $E_a^D$. Values are shown in Table 1. The average activation energy $E_a^D$ is ca. 170 kJ/mol, which lies in the range found for small molecule diffusion in rubbery polymers by Deppe et al. [37]. Values of $E_a^D$ are significantly larger than those of plasticizer transport in poly(vinyl chloride) [32] and ethylbenzene diffusion in polystyrene [38]. While such a large activation energy is surprising, it supports the premise that the interactions between the small molecule chemical functionality and the polymer have a strong impact on diffusion. The examples taken from Vergnaud [32] and Ventras and Duda [38] contain non-specific interactions between the small molecule and the polymer, unlike the present case in which the functional groups on the dopant can potentially interact with the polymer ester groups to retard diffusion and increase the activation energy.

A clear trend in the magnitude of $D$ does emerge: F > NF > DNF ≈ NP > TNF > CF, although with the caveat that the maximum difference in $D$ at any temperature is relatively small, at most two orders of magnitude. The range of diffusivity magnitudes seen here, $10^{-11}$ to $10^{-8}$ cm$^2$/s, are reasonable in the context of prior investigations, considering $T_g^{DSC} + 10 < T < T_g^{DSC} + 70$ °C. Diffusivities for small molecules in polymers typically range from $10^{-10}$ to $10^{-7}$ cm$^2$/s depending on the temperature relative to the polymer $T_g$ and the small molecule chemical structure [32,39,40]. Two primary factors affect diffusion: molecular size (and shape) [37] and intermolecular interactions. Small molecules diffuse through the free volume of the polymer, and can be assisted (or hindered) by segmental motion if there are sufficient interactions between molecule and polymer. In studies of ion [36] or water [41] diffusion, where coordination between transported species and polymer is very strong, changes in functionality can strongly modify the activation energy. Here, while the approximately constant activation energies suggest that the transport mechanism does not change dramatically between dopants, the trend in $D$ implicates functionality as playing a key role in retarding diffusion. As the interaction between the dopant functional group(s) and the polymer is strengthened, e.g., by adding nitro groups or exchanging a nitro for a cyano group, diffusivity is decreased. The cyano group forms stronger physical bonds than the nitro or carbonyl groups, as will be seen below in the plot of $K_C$. The similar values of $D$ for NP and NF, as

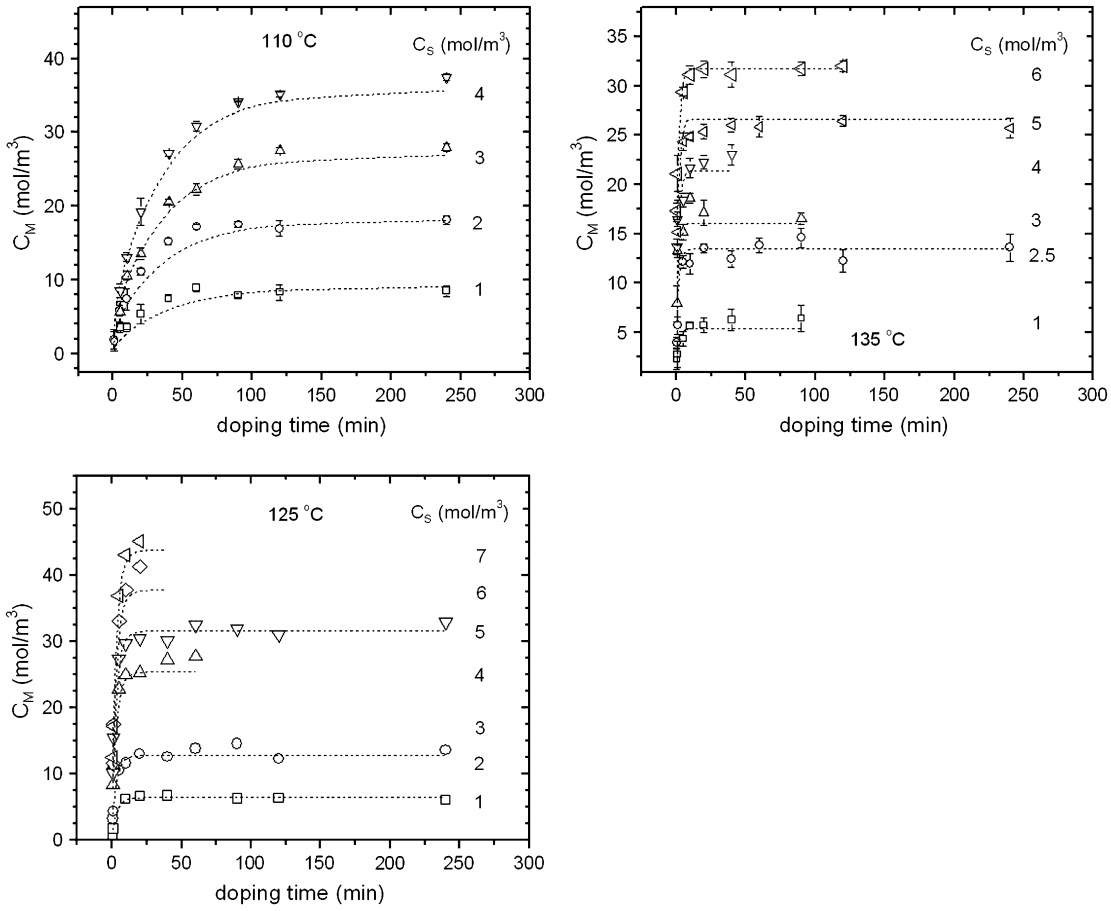


**Fig. 5.** Concentrations of DNF in Mylar® after doping at specified times, solution concentrations, and temperatures. Dashed lines indicate best-fits.

well as F possessing the highest diffusivity, also supports the importance of functionality in retarding diffusion.

Insight into the (lack of) impact of dopant size on the trends in Fig. 11 can be gained from estimations using the Einstein–Stokes relation. A sphere diffusing in a liquid has diffusivity $D \approx kT/6\pi\eta r$, where $k$ is Boltzmann's constant, $\eta$ is the polymer viscosity, and $r$ is the sphere radius. We obtain zero-shear viscosities from the relation in Gregory [42] and molecular radii from Table 2, assuming spherical molecules ($v_m^{d.P} = 4/3\pi(r_m^{d.P})^3$). Estimated values of $D$ are highly dependent on the Mylar® molecular weight and polydispersity index, which are unknown, but can be adjusted to place estimated values on the same scale as experimental values. As seen in Fig. 11, Einstein–Stokes predictions for F and TNF are barely distinguishable, the respectively smallest and largest fluorenones: the differences in the Einstein–Stokes predictions are tiny relative to the differences in experimental data. (Approximations are based on MW = 11,000 g/mol, $r_F = 3.98$ Å, and $r_{TNF} = 4.38$ Å. Changes to MW result in simple vertical shifts to all data.) In order to account for the approximate order of magnitude difference observed experimentally between F and TNF, $r_{TNF}$ would need to be 40 Å for the same $r_F$, an immense over-prediction. Therefore this comparison provides additional evidence for the importance of functionality over size in the diffusive transport of dopant.

As a final note on Fig. 11, the reason for the deviation of $D$ from the Arrhenius fit for CF at low temperatures is unknown. Measurement of $T_g$ for CF doped to 400 mol/m$^3$ (Fig. 6 in paper I) shows essentially no change from the undoped Mylar®, so plasticization of the PET is not responsible for an accelerated $D$.

### 4.3. Effective and actual diffusivities

Finally, the diffusivities $D$ measured here are in truth effective diffusivities. Due to the 39 ± 5% crystallinity of PET, small molecules follow a tortuous path through the amorphous phase around crystalline lamellae. By adopting a relationship for diffusion through porous catalyst to the present situation of diffusion through a semicrystalline polymer [43], we construct the true diffusivity $D_A$ as a function of the observed diffusivity $D$:

$$D = \frac{D_A \phi}{\tau} \tag{32}$$

where $\phi$ is the ratio of amorphous to total volume, and $\tau$ is the tortuosity or ratio of the actual distance a molecule travels between two points to the shortest distance between those two points. A constriction factor has been neglected because diffusion is relatively slow: there is no "pressure buildup" as in gaseous diffusion through porous catalysts. As a rough approximation, crystals will be considered as square obstructions in the diffusion path, giving $\tau = \sqrt{2}$, and the crystalline and amorphous densities [34] of PET are 1.515 and 1.335 g/cm$^3$, respectively. Accounting for the crystallinity therefore yields $D_A = 2.2D$.

### 4.4. Behavior of $K_C$: comparison between experiment and Flory–Huggins theory

The data series in Fig. 12 are distinctly separated with small error bars and provide several key insights into the doping behavior

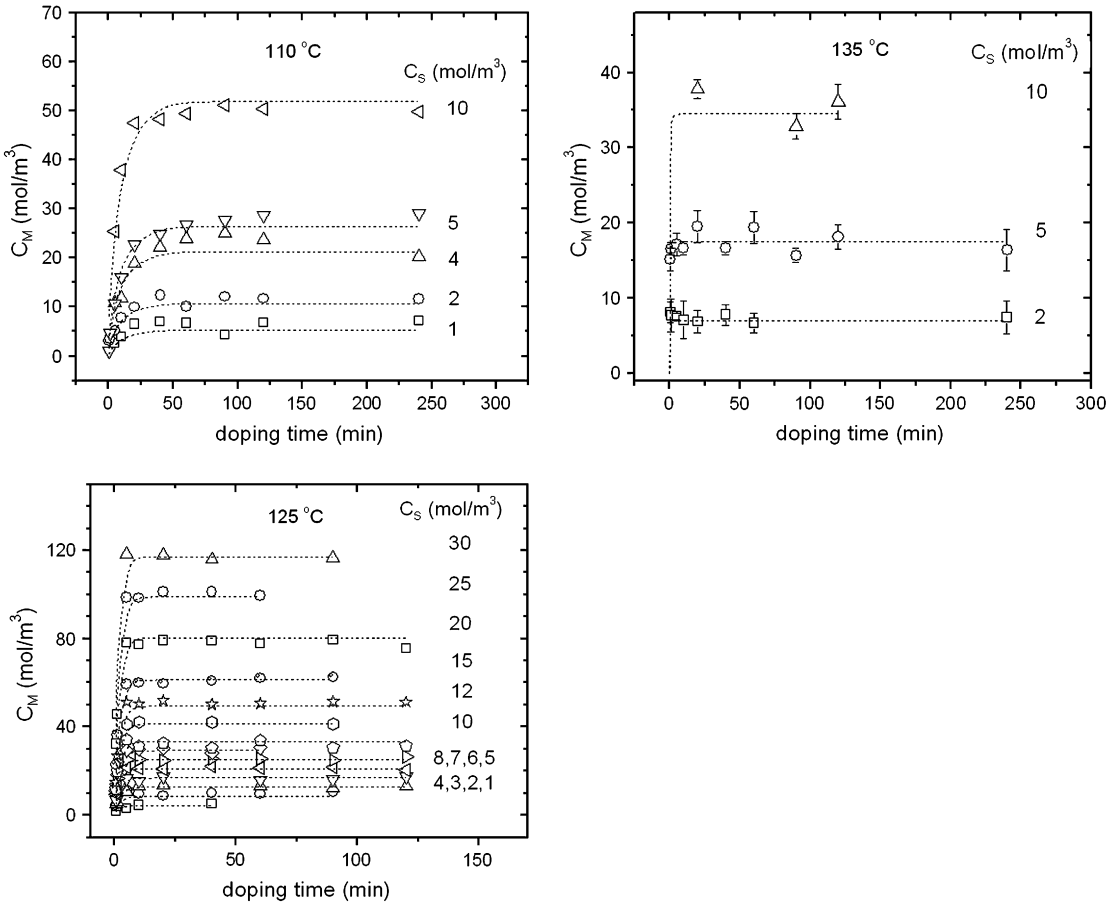


**Fig. 6.** Concentrations of NF in Mylar® after doping at specified times, solution concentrations, and temperatures. Dashed lines indicate best-fits.

of these materials. F, NF, DNF, and TNF are shifted in the direction of increasing number of nitro substituents, with small (but meaningful) changes in $E_a^K$. The data sets follow inverse Arrhenius behavior, as closely as can be determined with the limited number of points available. Previous studies [30,44] have found that in general, for a wide range of materials, experimentally determined values of $K_C$ follow inverse Arrhenius behavior, or

$$K_C(T) = K_{C\infty} \exp\left(E_a^K/RT\right) \tag{33}$$

Using the F–H theory (Eq. (25)), we can obtain the sign and magnitude of $E_a^K$ directly. F–H indicates it is based on a balance of solubilities: if $v_m^{d.S}(\delta_S - \delta_d)^2 > v_m^{d.P}(\delta_P - \delta_d)^2$, then $E_a^K > 0$. In the case of the fluorenones, PET, and EG, $v_m^{d.S}(\delta_S - \delta_d)^2$ is much larger than $v_m^{d.P}(\delta_P - \delta_d)^2$, explaining the inverse Arrhenius dependence observed in Fig. 12. It may be commented that in general, although the sign of $E_a^K$ may change depending on the solubility parameters, inverse Arrhenius behavior will be prevalently observed experimentally because doping is desired to progress in a strongly forward direction.

Specifically, values for $E_a^K$ can be predicted by the F–H model as follows. The solubility parameter $\delta$ for ethylene glycol has been reported within a wide range in the literature. Bandrup et al. [45] lists a value of 14.6 H, whereas solubility parameters originating from Hansen and Barton give 16.1 or 16.3 H [24,46]. Here we will select the Hansen solubility parameter of 16.1 H, as it seems to be the most recent and most widely used. (Units of H, the Hildebrand, are equivalent to $(cal/cm^3)^{1/2}$. H/0.489 [=] $MPa^{1/2}$.) Depending on the source, the estimated $\delta$ for PET ranges from 10.0 to 11.5 H, with the most common value of 10.7 H [20]. For the dopants we utilize the method developed by Smalls and refined by Fedors, which involves a ratio of the cohesive energy to the molar volume. Each atomic component contributes different values to the cohesive energy and molar volume, and these contributions are summed according to Eq. (24). This method provides values for the dopants as follows: $\delta_{TNF} = 13.4$ H, $\delta_{DNF} = 13.1$ H, $\delta_{NF} = 12.7$ H, $\delta_F = 12.2$ H, and $\delta_{CF} = 13.7$ H (accurate to approximately $\pm 0.4$). The trend in these values matches expectations that the addition of polar nitro or cyano groups will increase $\delta$.

For simple polymers such as polystyrene or polypropylene, the interaction site volume $v_m$ is typically assumed to be 100 Å$^3$ [15]. But it is known, from the crystal density (1.13 g/cm$^3$) and molecular weight ($M_0 = 180.21$ g/mol) of fluorenone, that a fluorenone molecule occupies, at minimum, 265 Å$^3$ or 159 cm$^3$/mol. Using this value for $v_m$ for both dopant in polymer and dopant in solvent provides a first estimate for the activation energy $E_a^K$, and for F it is relatively close to the experimental value: a theoretical value of 15 kJ/mol compared to an experimental value of 18 kJ/mol. However, as nitro groups are added, the theoretical trend falls in the wrong direction. Therefore, we use the experimental activation energies as a template to predict the actual $v_m$ values. In the polymer, there will be polar interactions between the dopant and the polymer, but there are no hydrogen bonds. In the solvent, however, there will be significant hydrogen bonding, and in the same way that hydration layers increase the volume of an ion in water [47], $v_m^{d.S}$ will increase due to hydrogen bonding solvent molecules. Therefore, we limit $v_m^{d.P}$ to calculated values, and allow $v_m^{d.S}$ to increase to the value predicted from Eq. (25) and the experimental $E_a^K$. Values for $v_m^{d.P}$ and $v_m^{d.S}$ are shown in Table 2. $v_m^{d.P}$ was estimated for F from the density and molecular weight, and the volume of additional substituents was added to obtain values for

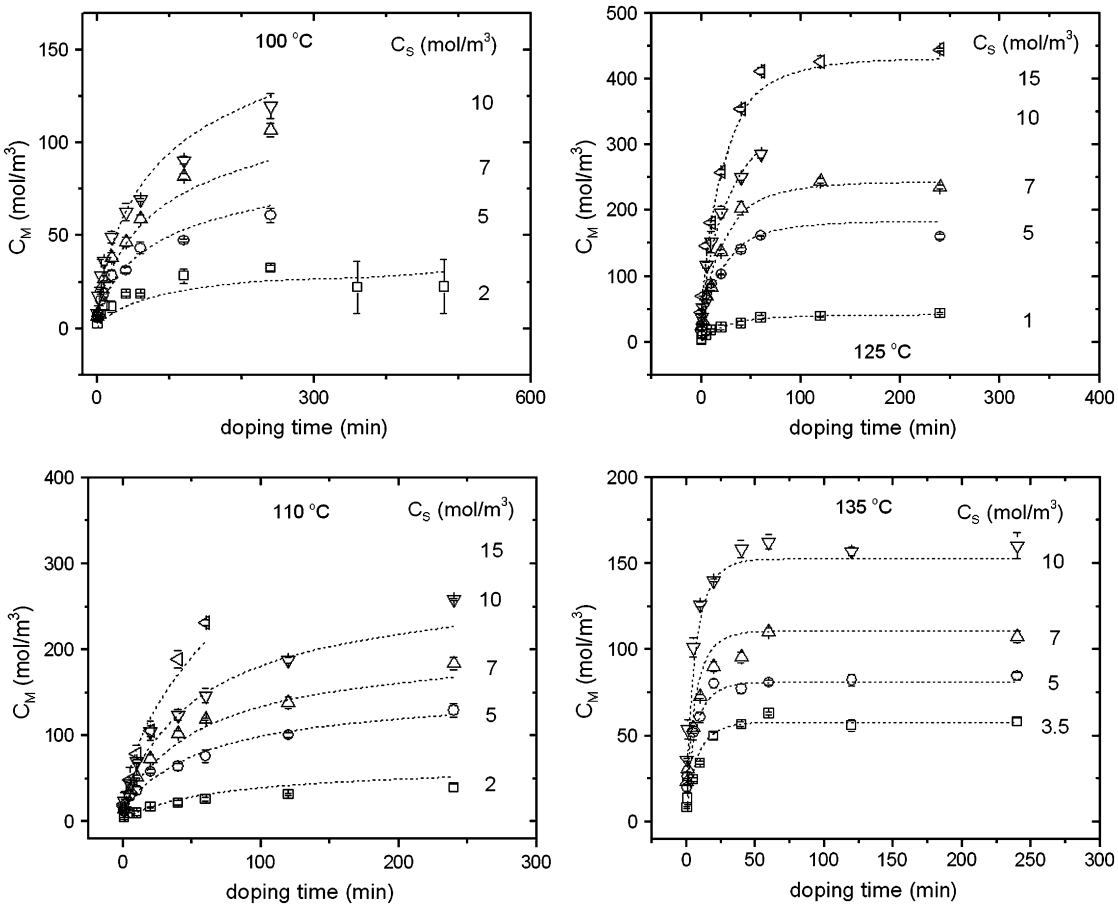


**Fig. 7.** Concentrations of CF in Mylar® after doping at specified times, solution concentrations, and temperatures. Dashed lines indicate best-fits.

$v_m^{d.P}$ for the other species. Volumes of a nitro group (~29 Å$^3$) and a cyano group (~10 Å$^3$) were calculated using atomic positions garnered from crystallographic data [48], and added linearly to the fluorenone volume to obtain molecular volumes for the other dopants.

Because F–H theory does not account for specific interactions outside of the $\chi$ parameters, it fails in the prediction of pre-exponential factors. The calculation proceeds (Eq. (17)) by finding values for $m_{d.S}$ and $m_{d.P}$ from molar volumes. For ethylene glycol, $M_0 = 62.07$ g/mol and $\rho = 1.13$ g/cm$^3$, giving 56.0 cm$^3$/mol. For PET, we can use the molecular weight of a single mer, provided the molar fraction $x$ or concentration $C$ is converted into molar fractions based on the same molecular weight. For PET, $M_0 = 192.1$ g/mol and $\rho_{amorph} = 1.335$ g/cm$^3$, giving 143 cm$^3$/mol of mers. Dopant volumes in the polymer $v_m^{d.P}$ and dopant volumes in the solvent $v_m^{d.S}$ are displayed in Table 2; resulting values of $m$ and F–H predictions for the pre-exponential are shown in the same table. The predicted pre-exponential is between 104 and 1011 times larger than the experimental value. The conversion between $K_C$ and $K_x$ of $K_C = K_x/2.57$ is accounted for in these calculations.

### 4.5. Corrections to F–H theory: impact of hydrogen bonding

As an example, the experimental value for $K_{C\infty}$ of fluorenone is 0.017, and the predicted value is 63. This extremely large discrepancy demonstrates the failure of Flory–Huggins theory, which arises from the fact that F–H theory is based on dispersive forces and therefore depends solely on molar fractions and volumetric considerations (with the exception of contributions from the experimental $\chi$ parameter). Specifically, the influence of hydrogen bonds will be to decrease $\gamma_d^S$ and therefore decrease the pre-exponential term for $K_C$. Explicit values cannot be obtained from the hydrogen bonding model of Panayiotou and Sanchez (Eq. (20)), because full thermodynamic data on the system are not available, but it is possible to show that the impact of the hydrogen bonding-based contribution to the activity coefficient, $\gamma_d^{S(H)}$, will be to significantly decrease the pre-exponential factor in Eq. (17), and in turn use relation for hydrogen bonding to approximate the number of hydrogen bonds per molecule. The simplified relation (which is very approximate) of Eq. (21) has an exponential dependence on $-2a$, and can therefore decrease the predicted $K_{C\infty}$ significantly.

In the case of EG solvating a larger dopant molecule such as flourenone, it may be expected that a single dopant molecule will be coordinated by multiple EG molecules simultaneously, or $a > 1$. The values of $a$ obtained from Eq. (21) and indicated in Table 2 range from 4 and 13 H-bonds per dopant molecule, increasing in the trend of more nitro groups and more polar dopant molecules. Assuming that each EG molecule provides between one and two H-bonds, the volumes of the EG-coordinated dopant molecules can be estimated, as a check to the calculated values of $v_m^{d.S}$ (where EG has the molar volume 55.98 cm$^3$/mole as calculated earlier). The range provided from these calculations obtained from predicted $a$ values are close to or encompass values of $v_m^{d.S}$, demonstrating that the method developed here is at least self-consistent, and at best provides a physically meaningful interpretation of the data.

The calculations described thus far, although obtaining physically realistic values for F, NF, DNF, and TNF, do not make sense for CF. There were several difficulties in the experimental evaluation of $C_M(t)$ for CF, including: the UV absorbance for CF is weak, making

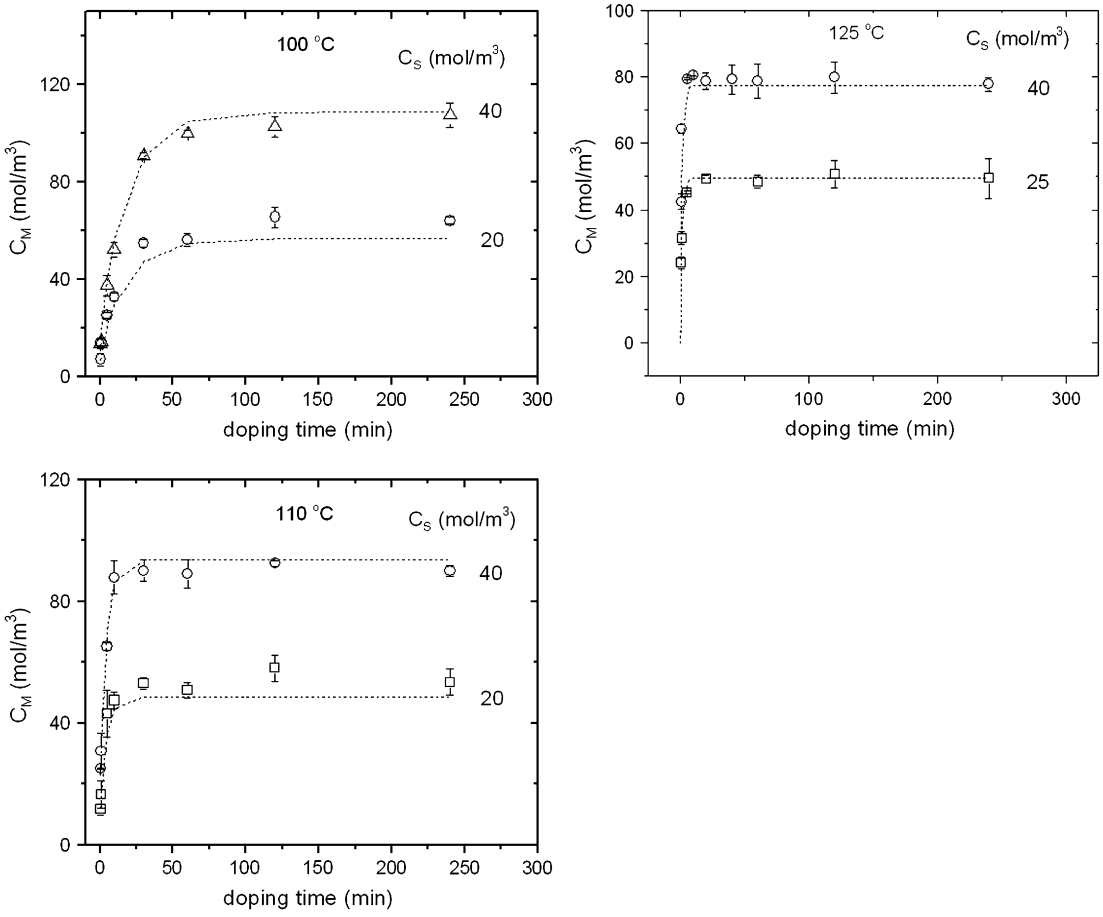


**Fig. 8.** Concentrations of F in Mylar® after doping at specified times, solution concentrations, and temperatures. Dashed lines indicate best-fits.

concentration calculations difficult; CF solutions changed color at elevated temperatures quickly, indicating degradation of the dopant; and there was a limited amount of the chemical commercially available. These factors could potentially skew the equilibrium concentration data, resulting in deviations from the theory in this paper; or the approach utilizing the solubility parameters and modified F–H theory may omit some critical interaction(s) that occur between the cyano group and the solvent and polymer. Either way, the theory outlined here does not predict experimental observations with CF, and further calculations in Table 2 are omitted. Future investigations should obtain more data and establish a better theoretical understanding of the behavior of cyanofluorenone.

### 4.6. Implications of Flory–Huggins theory

With the previous calculations in hand, we can begin to understand the physical situation and the reasons for the observed level of doping. First, the differences in solubility parameters – $\delta$ of the dopant (~12.2 H) being closer to that of the polymer (10.7 H) than that of ethylene glycol (16.1 H) – are the primary driving forces for partitioning of a high fraction of the dopant into the polymer. The second driving force is the influence of the dopant site interaction volume, larger in the solvent than in the polymer due to H-bonding as described above, also plays a significant role in the magnitude of $E_a^K$. The third contribution is the enthalpic energy of hydrogen bonding: the over-estimated pre-exponential values from F–H theory must arise from hydrogen bonding between EG and the dopant. Before continuing to the application of UNIFAC for $K_C$, however, it is beneficial to consider the use of solubility parameters in extending $K_C$ predictions to a wider range of solvents. We postulated in a prior work [3] that solubility parameter did not appear to be the determining factor when doping Mylar® from a variety of solvents. However, this conclusion was based on a smaller value of $\delta$ for EG. Using $\delta_{EG} = 16.1$ H, the doping trends appear to fall into excellent agreement with the trend in solubility parameter, once dopant volumes have been accounted for. This is exhibited in Fig. 13 for four dopants and nine solvents, for the same doping conditions: $C_S = 2$ mol/m$^3$ and $T = 100$ °C. (Two other dopants, anthracene and phenazine, also demonstrated excellent agreement between theory and experiment, but were removed from the plot for clarity.) Importantly, this predicts the behavior of TCQM and TNF observed in our previous work [3]:

TCQM was observed to dope well from low $\delta$ solvents, whereas TNF doped best from EG, a high $\delta$ solvent. The correlation due to solubility parameter differences and interaction site volumes, although requiring two adjustable parameters to match the magnitudes of $C_M$, follows the trends as a function of solvent solubility with very few outliers. The relation used to fit the data was

$$C_M = a_1 \exp\left\{b_1\left[v_m^{d,S}(\delta_S - \delta_d)^2 - v_m^{d,P}(\delta_P - \delta_d)^2\right]\right\} \quad (34)$$

where $a_1$ and $b_1$ are adjustable parameters specific to each dopant. Values for $v_m^{d,S}$ (in the hydrogen bonding solvents only) were estimated by assuming three hydrogen bonds per nitro or cyano group, with the corresponding increase to the un-coordinated dopant

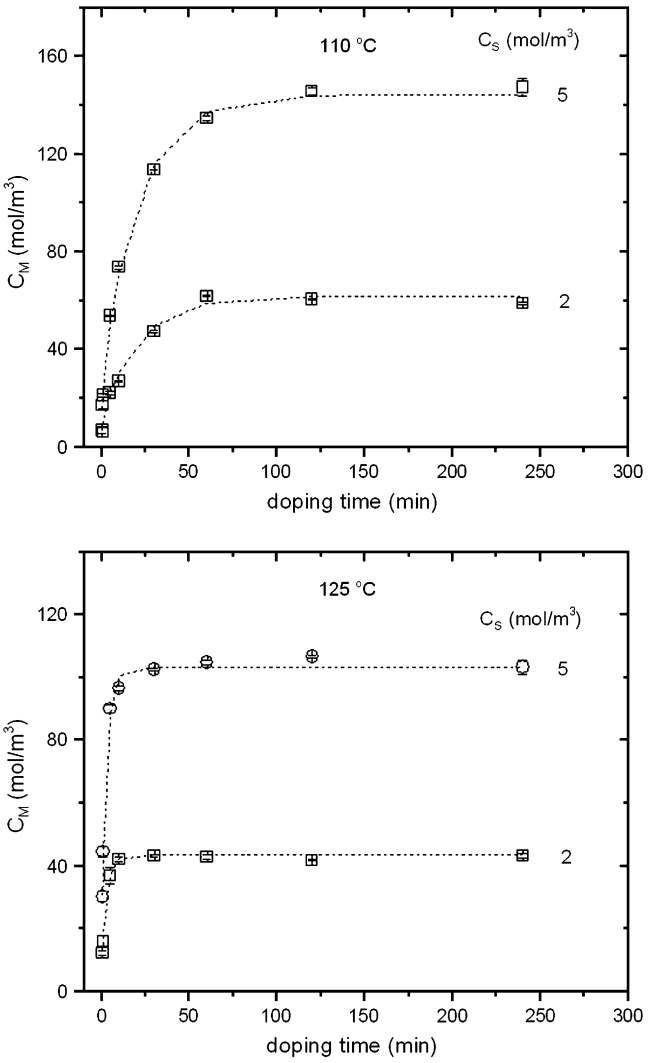


**Fig. 9.** Concentrations of NP in Mylar® after doping at specified times, solution concentrations, and temperatures. Dashed lines indicate best-fits.

volume $v_m^{d,P}$, which was calculated from crystal density and molecular weight. The excellent correlations in Fig. 13 for a wide range of chemistry demonstrate that, although not quantitative in terms of the magnitude of $C_M$ without adjustable parameters, the use of $\chi$ and $\delta$ parameters is extremely valuable in qualitatively assessing trends in doping as a function of dopant, solvent, and polymer chemistry.

### 4.7. Predictions of UNIFAC

For all the recent modifications to F–H theory to account for hydrogen bonding, UNIFAC, which is based on interactions between functional groups, does not contain terms representative of hydrogen bonds. This is a serious problem, since ethylene glycol will hydrogen bond very strongly with the carbonyl, nitro, and cyano groups of the fluorenone molecules being considered, as discussed above. UNIFAC does, however, represent polar interactions well. Fig. 14 represents calculations of the UNIFAC program developed by Sandler [49], for F, NF, and DNF. Since this program does not contain parameters to represent interactions between ethylene glycol O–H groups and C═O or $NO_2$, ethylene glycol is instead represented as O═CH–CH═O. For the same reason, aromatic C–$NO_2$ groups are replaced by CH–$NO_2$ groups.

Surprisingly, the UNIFAC predictions shown in Fig. 14 are completely contrary to experimental data, in both magnitude and trend as a function of dopant chemistry. The balance of interactions between nitro groups and solvent and nitro groups and polymer is predicted to strongly favor the dopant remaining in the polymer. There is critical information lost in the UNIFAC model, presumably because of its inability to account for hydrogen bonding in the liquid. This information is of course contained in the $\chi$ parameters, making the method utilizing $\chi$ parameters (Eq. (17)) with corrections for H-bonds (Eq. (20)) the most suitable for estimating the partition coefficient $K_C$.

## 5. Summary

Small molecule concentrations obtained from the doping of Mylar® with electron traps were fit to high precision using the combined partition–diffusion model, with all coefficients of determination $R^2$ greater than 0.975.

Diffusivity $D$ was observed to follow the Arrhenius relation for all dopants investigated (with the exception of CF at low $T$), which is typical for small molecule diffusion sufficiently above $T_g$. The trend in $D$ was: F > NF > DNF ≈ NP > TNF > CF, although the maximum difference in $D$ at any temperature between dopants is only two orders of magnitude. Within the measurement error, all dopants exhibit approximately the same activation energy, and this indicates that the same transport mechanism is relevant to each dopant. Conclusive evidence as to the balance of size versus functionality on diffusivity is not available given the limited number of dopants, but the trends in $D$ and comparison with predictions of the Einstein–Stokes relation support dopant functionality over size as the primary factor leading to the observed differences in $D$. Based on the data for CF, F, NF, and NP, strong interactions act to retard diffusivity, while at the same time enhancing the equilibrium concentration within the film. The bulk (measured) diffusivity is a fraction of the true diffusivity, due to the fact that essentially no dopant penetrates the tightly-packed crystalline domains. Accounting for the crystallinity of $39 \pm 5\%$ and the tortuous path required for diffusion around the crystalline domains, the true diffusivity is approximately 2.2 times the measured diffusivity.

Values of the equilibrium partition coefficient $K_C$ formed distinct trends for each dopant chemistry and provided several key insights into the doping process, especially upon analysis of the data in the context of modified Flory–Huggins theory. First, the data sets follow inverse Arrhenius behavior, which may be explained by the magnitude of the solubility parameters and interaction volumes. As $v_m^{d,S}(\delta_S - \delta_d)^2$ is significantly larger than $v_m^{d,P}(\delta_P - \delta_d)^2$, $K_C$ follows inverse Arrhenius temperature dependence and the dopant partitions heavily from the solvent into the polymer phase. Second, knowledge of the solubility parameters, interaction volume $v_m^{d,P}$, and activation energy $E_a^K$ allows for calculation of the interaction volume $v_m^{d,S}$, which is larger than $v_m^{d,P}$ by virtue of the hydrogen-bonded EG molecules surrounding the dopant in solution. Third, experimental values for $E_a^K$ and $K_C$ and calculated values for the F–H pre-exponential provide estimates for the average number of hydrogen bonds per dopant molecule. Consistency was observed between the calculated $v_m^{d,S}$ from both methods (originating separately from exponential and pre-exponential), therefore supporting the validity of the analysis. Hydrogen bonding increases with the number of polar substituents on the dopant, from about four for F to about 13 for TNF.

A significant success to the method utilizing solubility parameters was indicated by the ability to predict trends in equilibrium dopant concentration for a variety of dopants and solvents. This method provides a theoretical understanding for, e.g., the observed

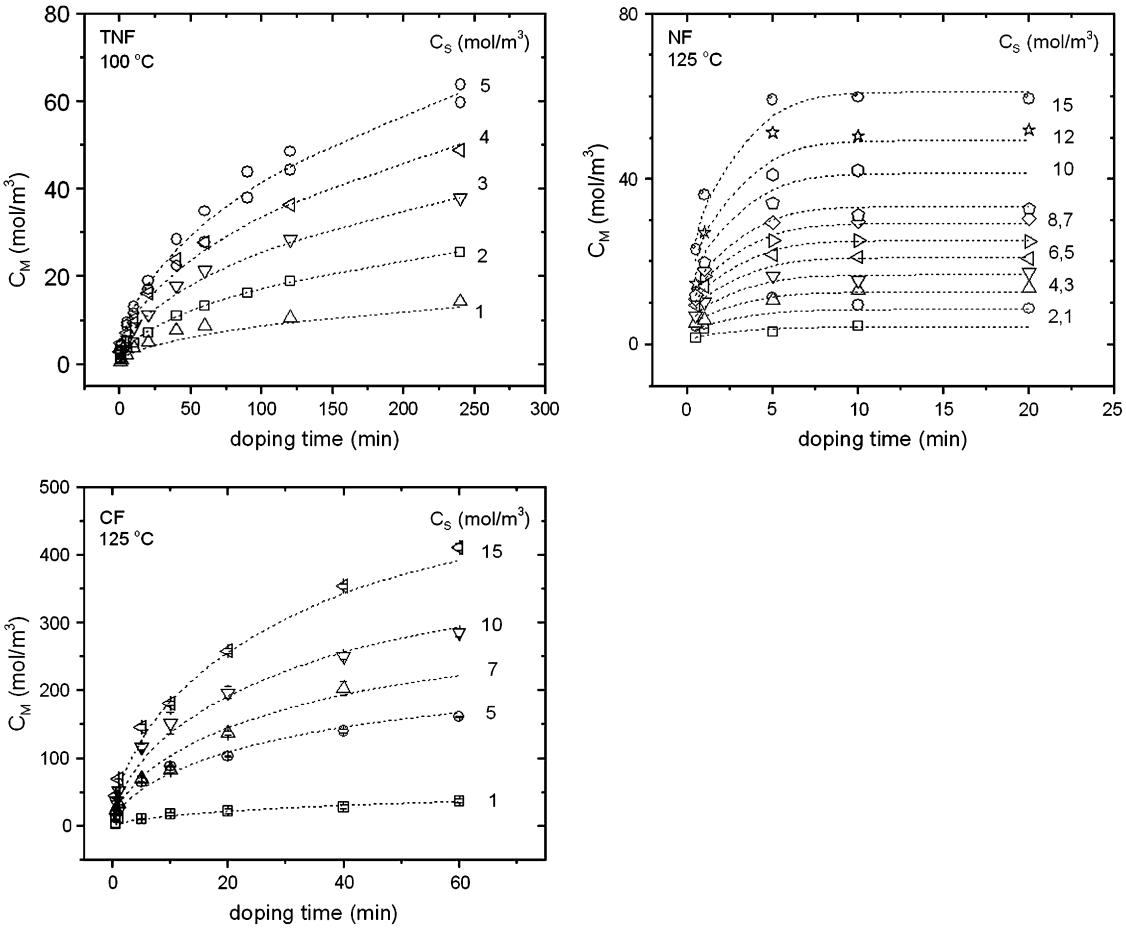


**Fig. 10.** Concentrations in Mylar® of selected dopants and temperatures as a function of time and solution concentration, shown at short times to clarify the preceding figures. Dashed lines indicate best-fits.

strong doping behavior of TNF from EG and poor doping behavior of TCQM from EG. It also predicts enhanced doping for the fluorenones from glycerin (glycerol) as the solvent over EG, which was confirmed experimentally using DNF.

Two surprising failures were uncovered in this study. First, UNIFAC, based on group contribution theory, did not accurately

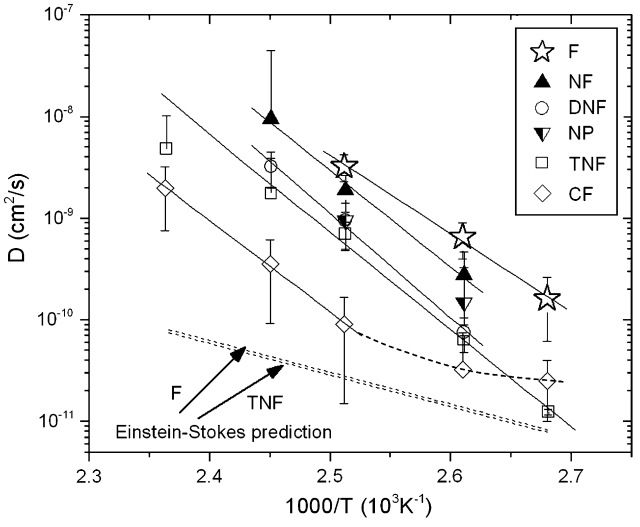


**Fig. 11.** Arrhenius plot of diffusivity $D$ for the dopants diffusing in PET. Straight solid lines indicate best-fits. Straight dashed lines represent predictions based on the Einstein–Stokes relation.

**Table 1**
Parameters obtained from fitting Arrhenius and inverse Arrhenius relations to diffusivity $D$ and equilibrium adsorption constant $K_C$, respectively

| Dopant | $D_\infty$ (cm$^2$/s) | $E_a^D$ (kJ/mol) | $K_{C\infty}$ | $E_a^K$ (kJ/mol) |
|---|---|---|---|---|
| F | $8 \times 10^{10}$ | 150 | 0.02 | 18 |
| NF | $2 \times 10^{15}$ | 180 | 0.007 | 22 |
| DNF | $6 \times 10^{16}$ | 200 | 0.002 | 23 |
| TNF | $6 \times 10^{14}$ | 180 | 0.001 | 25 |
| CF | $4 \times 10^{12}$ | 170 | $4.0 \times 10^{-9}$ | 91 |

Parameter errors are estimated to be 100% for pre-exponential factors and 20% for activation energies.

**Table 2**
Experimental, theoretical, and calculated parameters resulting from data and theory for dopant partitioning

| Dopant | $v_m^{d.P}$ (Å$^3$) | $v_m^{d.P}$ (cm$^3$/mol) | $E_a^K$ (expt, kJ/mol) | $\delta d$ (H) | $v_m^{d.S}$ (cm$^3$/mol) | $m_{d.S}$ |
|---|---|---|---|---|---|---|
| F | 265 | 159 | 18 | 12.2 | 312 | 5.6 |
| NF | 294 | 177 | 22 | 12.7 | 520 | 9.3 |
| DNF | 323 | 195 | 23 | 13.1 | 729 | 13 |
| TNF | 352 | 212 | 25 | 13.4 | 1040 | 19 |
| CF | 275 | 166 | 91 | 13.7 | – | – |

| Dopant | $m_{d.P}$ | $K_{C\infty}^{F-H}$ | $K_{C\infty}^{expt}$ | $a$ | $v_m^{d.S}$(I, cm$^3$/mol) | $v_m^{d.S}$(II, cm$^3$/mol) |
|---|---|---|---|---|---|---|
| F | 1.1 | $1.7 \times 10^2$ | 0.017 | 4 | 420 | 290 |
| NF | 1.2 | $9.2 \times 10^3$ | 0.0069 | 7 | 570 | 370 |
| DNF | 1.4 | $4.4 \times 10^5$ | 0.0018 | 10 | 740 | 470 |
| TNF | 1.5 | $1.3 \times 10^8$ | 0.0013 | 13 | 920 | 570 |
| CF | – | – | $3.5 \times 10^{-9}$ | – | – | – |

Variables are defined in the text; expt indicates experimental, F–H indicates Flory–Huggins theory, and I and II indicate calculations using $a$ and $a/2$, respectively. Errors for the molar volumes $v_m$, volume ratios $m$, solubility parameters $\delta_D$, and activation energies $E$ are approximately ±5%; errors for the other parameters are approximately ±25%.

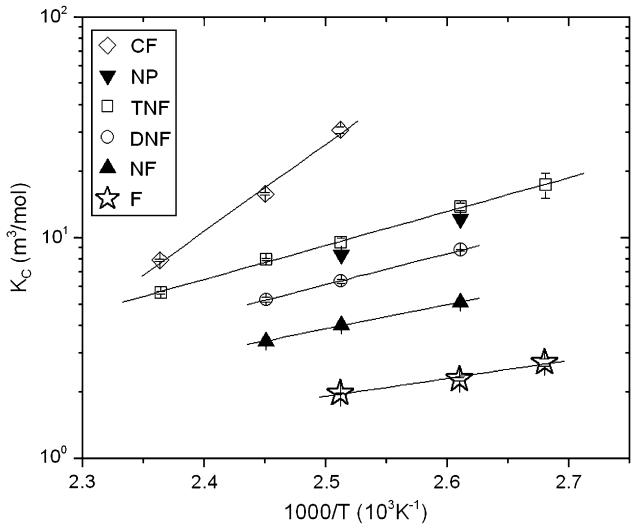


**Fig. 12.** Arrhenius plot of equilibrium adsorption constant $K_C$ for dopants adsorbing to PET. For PET and EG, $K_x = 2.57K_C$, in terms of the PET mer molecular weight. Lines indicate best-fits.

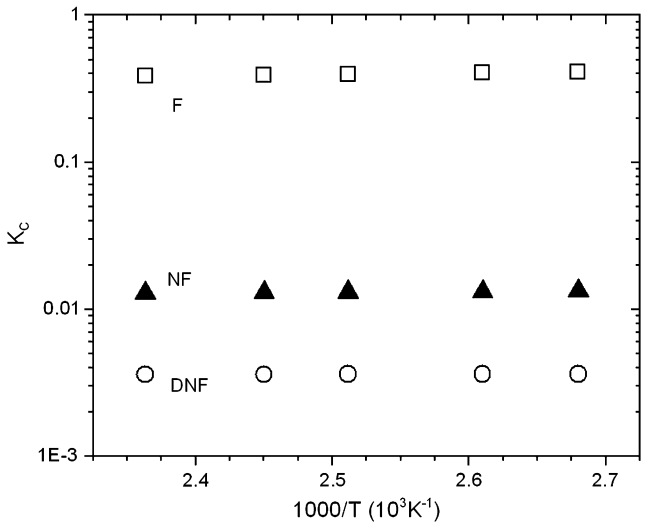


**Fig. 14.** Values of $K_C$ (T) estimated from the UNIFAC method.

predict either the magnitude or temperature dependence of the partition coefficient, likely because of its inability to account for hydrogen bonding. Second, the behavior of $K_C$ for CF was abnormal relative to the other molecules, and the method based on solubility parameters, F–H theory, and hydrogen bonding failed to account for the behavior of the experimental data arising from the addition of a single cyano group.

### 5.1. Key points

There are several key conclusions, reached from the data in papers I and II, which have broad implications for the doping of polymers from solution.

1) Transport in the glassy phase is restrictively slow. The polymer must be above its $T_g^{DSC}$ by at least 20–30 °C to allow diffusion to penetrate a 12.9 μm film on a reasonable (<20 h) time scale.

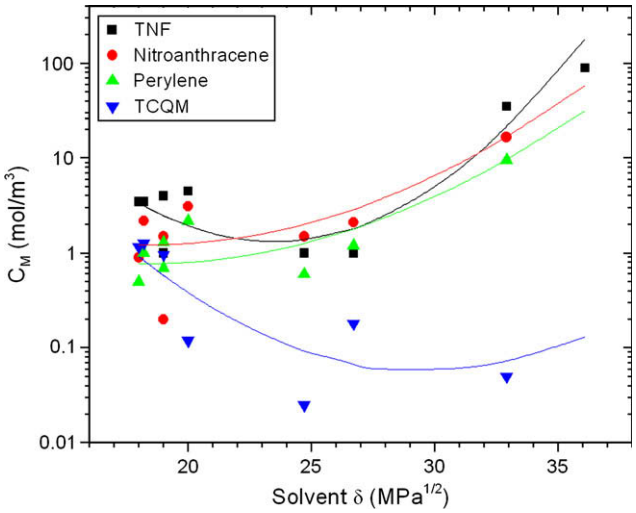


**Fig. 13.** Experimental data (points) and fits (lines) of $C_M$ as a function of solvent solubility parameter. Fits are based on the dopant, solvent, and polymer solubility parameters, as well as the approximated dopant volumes, with two adjustable parameters (Eq. (34)). All points represent 100 °C, 2 mol/$m^3$, and >4 h, with errors of ~5% in $C_M$.

2) Based on the excellent fits of $C_M(t,T)$ and the consistency between theory and experiment for $D$ and $K_C$, critical assumptions about the diffusion and partitioning processes appear to hold for these studies: (a) diffusion is not enhanced through plasticization by the dopant or solvent; and (b) the equilibrium concentration is sufficiently low that dopant molecules do not distort the thermodynamics of the polymer matrix (with the possible exception of CF).
3) Both diffusion and partitioning are strongly affected by the chemical functionality of the dopant and the resulting specific interactions between the solvent, polymer, and dopant. Diffusion is significantly retarded upon the addition of chemical functionality to the dopant molecule, with increased polarity leading to lower diffusivities. The partition coefficient is generally enhanced by increased polarity of the dopant molecule.
4) The solubility parameters, in combination with estimations for the local interaction volumes, provide an excellent method to predict trends in the equilibrium doping behavior via the $\chi$ parameter and F–H theory, for a variety of chemistries.

## Acknowledgements

Sandia is a multiprogram laboratory operated by Sandia Corporation, a Lockheed Martin Company, for the United States Department of Energy's National Nuclear Security Administration under contract DE-AC04-94AL85000. Thanks to Mark Stavig for assistance with the DMA and DSC.

## References

[1] Kurtz SR, Hughes RC. Journal of Applied Physics 1983;54:229.
[2] Kurtz SR, Arnold JC. Journal of Applied Physics 1985;57:2532.
[3] Lenhart JL, Cole PJ, Schroeder JL, Cole SM, Belcher M, Baum N. Journal of Applied Physics 2008;103:024908.
[4] Klein RJ, Schroeder JL, Cole SM, Belcher ME, Cole PJ, Lenhart JL. Polymer 2008;49:2632.
[5] Klein RJ, Cole SM, Belcher ME, Schroeder JL, Cole PJ, Lenhart JL. Polymer 2008; 49:5541.
[6] Dill KA. Journal of Physical Chemistry 1987;91:1980.
[7] De Young LR, Dill KA. Journal of Physical Chemistry 1990;94:801.
[8] Vig JR. Journal of Vacuum Science and Technology A – Vacuum Surfaces and Films 1985;3:1027.
[9] Klein RJ, Fischer DA, Lenhart JL. Langmuir 2008;24:8187.
[10] Smith JM, Van Ness HC, Abbott MM. Introduction to chemical engineering thermodynamics. New York: McGraw-Hill; 1996. p. 315–60.

[11] Sandler SI. Chemical and engineering thermodynamics. New York: John Wiley and Sons, Inc.; 1989. p. 305–74.
[12] Smith JM, Van Ness HC, Abbott MM. Introduction to chemical engineering thermodynamics. New York: McGraw-Hill; 1996. p. 366–414.
[13] Sanchez IC, Lacombe RH. Macromolecules 1978;11:1145.
[14] Panayiotou C, Sanchez IC. Journal of Physical Chemistry 1991;95:10090.
[15] Rubinstein M, Colby RH. Polymer physics. New York: Oxford University Press; 2003. p. 137–65.
[16] Wakahayashi T, Oki S, Omori T, Suzuki N. Journal of Inorganic and Nuclear Chemistry 1964;26:2255.
[17] Miller-Chou BA, Koenig JL. Progress in Polymer Science 2003;28:1223.
[18] Graf JF, Coleman MM, Painter PC. Journal of Physical Chemistry 1991;95:6710.
[19] Atorngitjawat P, Klein RJ, Runt J. Macromolecules 2006;39:1815.
[20] Van Krevelen DW. Properties of polymers: their correlation with chemical structure; their numerical estimation and prediction from additive group contributions. New York: Elsevier Science Publishing Company; 1990. p. 189–225.
[21] Small PA. Journal of Applied Chemistry 1953;3:71.
[22] Fedors RF. Polymer Engineering and Science 1974;14:147.
[23] Fedors RF. Polymer Engineering and Science 1974;14:472.
[24] Barton AFM. Handbook of solubility parameters. CRC Press; 1983. p. 153–7.
[25] Fredenslund A, Gmehling J, Michelsen ML, Rasmussen P, Prausnitz JM. Industrial and Engineering Chemistry Process Design and Development 1977;16:450.
[26] Larsen BL, Rasmussen P, Fredenslund A. Industrial and Engineering Chemistry Research 1987;26:2274.
[27] Fredenslund A, Rasmussen P. Fluid Phase Equilibria 1985;24:115.
[28] Gmehling J, Lohmann J, Jakob A, Li J, Joh R. Industrial and Engineering Chemistry Research 1998;37:4876.
[29] Tiegs D, Rasmussen P, Gmehling J, Fredenslund A. Industrial and Engineering Chemistry Research 1987;26:159.
[30] Vergnaud JM. Liquid transport processes in polymeric materials: modeling and industrial applications. New Jersey: Prentice-Hall, Inc.; 1991. p. 45–61.
[31] Barrer RM. Journal of the Chemical Society 1951:1874–6.
[32] Vergnaud JM. Liquid transport processes in polymeric materials: modeling and industrial applications. New Jersey: Prentice-Hall, Inc.; 1991. p. 116–9.
[33] Bird RB, Stewart WE, Lightfoot EN. Transport phenomena. New York: John Wiley and Sons; 1960. p. 352–70.
[34] Kong Y, Hay JN. Polymer 2002;43:3873.
[35] Ratner MA. In: MacCallum JR, Vincent CA, editors. Polymer electrolyte reviews, vol. 1. New York: Elsevier Applied Science; 1987.
[36] Klein RJ, Zhang SH, Dou S, Jones BH, Colby RH, Runt J. Journal of Chemical Physics 2006:124.
[37] Deppe DD, Miller RD, Torkelson JM. Journal of Polymer Science Part B: Polymer Physics 1996;34:2987.
[38] Vrentas JS, Duda JL. Journal of Polymer Science Part B: Polymer Physics 1977;15:417.
[39] Krongauz VV, Mooney WF, Schmelzer ER. Polymer 1994;35:929.
[40] Aminabhavi TM, Phayde HTS, Dale Ortego J, Vergnaud JM. Polymer 1996;37:1677.
[41] Soles CL, Chang FT, Gidley DW, Yee AF. Journal of Polymer Science Part B: Polymer Physics 2000;38:776.
[42] Gregory DR. Journal of Applied Polymer Science 1972;16:1489.
[43] Fogler HS. Elements of chemical reaction engineering. 3rd ed. Upper Saddle River, New Jersey: Prentice Hall PTR; 1999. p. 738–41.
[44] Fogler HS. Elements of chemical reaction engineering. 3rd ed. Upper Saddle River, New Jersey: Prentice Hall PTR; 1999. p. 594–618.
[45] Brandrup J, Immergut EH, Grulke EA, editors. Polymer handbook. 4th ed. New York: John Wiley and Sons, Inc.; 1999. p. V–114.
[46] Hansen CM. Journal of Paint Technology 1967:39.
[47] Bockris JO, Reddy AKN. Modern electrochemistry 1: ionics. New York: Plenum Press; 1998. p. 35–87.
[48] O'Bannon PE, Carroll PJ, Dailey WP. Structural Chemistry 1991;2:133.
[49] Sandler SI. Chemical and engineering thermodynamics. New York: John Wiley and Sons, Inc.; 1989. p. 381–487.